GRICP: Granular-Ball Iterative Closest Point with Multikernel Correntropy for Point Cloud Fine Registration

Yihao[1], Limei Hu[1], Feng Chen[1*], Sen Zhao[2,3], Shukai Duan[1]

[1]College of Artificial Intelligence, Southwest University, Chongqing, China
[2]Key Laboratory of Big Data Intelligent Computing
[3] Chongqing University of Telecommunications and Posts, Chongqing, China
{little1shaow,fengchen.uestc}@gmail.com, {hlm0903,duansk}@swu.edu.cn, zhaosen@cqupt.edu.cn

Abstract

The Iterative Closest Point (ICP) algorithm suffers from sensitivity to outliers and tendency to local optima in point cloud fine registration. In this paper, we introduce a global and robust ICP framework called Granular-Ball Iterative Closest Point with MultiKernel Correntropy (GRICP). This approach transforms the point cloud into a granular ball cloud and employs MultiKernel Correntropy (MKC) as the loss function, which is designed to smooth out the effects of noise points and provide global information for registration. Specifically, we propose a coarse-grained representation of the point cloud using the granular ball model, which adaptively captures the coarse-grained features of the data and converts the point cloud into a multi-granularity ball cloud. The normal points within each granular ball help mitigate the influence of noise points. To ensure that ICP finds the globally optimal transformation, MKC is introduced to measure the distribution of registration errors, thereby offering global insights for ICP to achieve the optimal solution. The transformations based on MKC and the granular ball cloud are then derived. Extensive experiments on both simulated and real-world datasets demonstrate that GRICP delivers superior registration performance, particularly in scenarios involving large rotation offsets, partial overlaps, and Gaussian noise.

Introduction

Point cloud fine registration techniques are widely used in 3D scene reconstruction (Agarwal et al. 2011), autonomous driving (Bresson et al. 2017), and robotics (Durrant-Whyte and Bailey 2006). The goal of point cloud fine registration is to accurately align two point clouds by finding a rigid transformation.

A classic work in the field is the Iterative Closest Point (ICP) algorithm (Besl and McKay 1992), which aligns two point clouds iteratively until convergence by matching points based on spatial proximity and then solving a least-squares problem for the transformation. ICP is extremely sensitive to noise and initial conditions and tends to get stuck in suboptimal solutions. To improve the robustness of ICP to noise, robust loss functions have been introduced in previous works (Bouaziz, Tagliasacchi, and Pauly 2013), (Wu et al. 2019), (Liu, Pokharel, and Principe 2007) to reduce the influence of noise points. These methods are based on Gaussian kernel functions, and the choice of kernel width greatly affects the results. To avoid the issue of kernel width selection, a symmetric objective function for ICP was proposed in (Li et al. 2022) and (Rusinkiewicz 2019). Nevertheless, the inclusion of a symmetric objective function can slow down the convergence of ICP. To address this, Anderson acceleration (Anderson 1965) was introduced to speed up convergence, as discussed in (Pavlov et al. 2018) and (Zhang, Yao, and Deng 2021). Despite this, the approach adds extra computational burden during optimization. To address the drawback of ICP's tendency to fall into local optima, Global ICP (Go-ICP) (Yang et al. 2015) and its variants based on the branch-and-bound method have been proposed. A major limitation of these methods is that they are highly time-consuming when applied to large-scale point clouds. To achieve global optimization while maintaining efficiency, neural network-based methods such as Deep Closest Point (DCP) (Wang and Solomon 2019) have been introduced. These methods utilize transformers to extract high-dimensional features of points, generating high-quality initial correspondences.

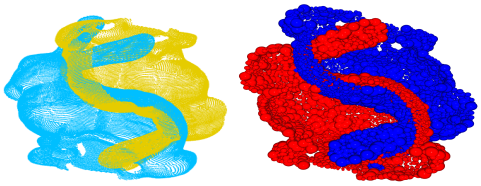

(a) (b)

Figure 1: (a): the original point clouds. (b): the corresponding granular ball cloud.

In this paper, we propose a global and robust Iterative Closest Point method for fine registration of point clouds. By transforming the point cloud into a granular ball cloud (Xia, Xie, and Wang 2022) and introducing MultiKernel Correntropy (MKC) (Chen et al. 2021) as the loss function, we achieve globally robust fine registration. Specifically, our model mainly consists of two stages.

First, we transform the point cloud into a granular ball cloud. The majority of normal points within each granular ball can smooth out the influence of a few noise points while

*Corresponding author
Copyright © 2025, Association for the Advancement of Artificial Intelligence (www.aaai.org). All rights reserved.

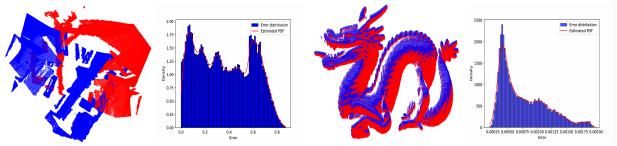

(a) (a) (b) (b)

Figure 2: (a): Error distributions when the algorithm is trapped in a local optimum. (b): Error distribution for global registration.

effectively preserving the shape of the point cloud, as shown in Fig. 1. This is due to the fact that granular balls are an adaptive clustering model capable of effectively capturing the coarse-grained information of the point cloud in different regions (Xie et al. 2024c). The radius and density of the balls, along with their overlap with neighbors, can be considered coarse-grained features (Zhang et al. 2023). These features are useful for subsequent outlier rejection steps. Additionally, the number of granular balls is significantly lower than the number of points, reducing the computational burden of the method (Cheng et al. 2023). For the issue of local optima, we observed that when ICP falls into local minima, the error tends to exhibit a multi-peak distribution, as illustrated in Fig.2. Loss functions that assume a single distribution (e.g., Gaussian kernel functions (Liu, Pokharel, and Principe 2007)) find it challenging to handle such multi-peak error distributions. Consequently, we utilize MultiKernel Correntropy (MKC) (Chen et al. 2021), which can rapidly assess the error distribution at each iteration. By employing MKC as the loss function in ICP, we derive the rigid transformation accordingly.

Based on the aforementioned insights, we propose an efficient and lightweight point cloud registration framework to address the challenges of local optima and robustness, named Global Robust Iterative Closest Point (GRICP). The main contributions are:

- To address local optima in ICP, Multi-Kernel Correntropy (MKC) is introduced as a loss function to incorporate global information. This function is integrated into ICP, leading to updated expressions for R and t based on MKC.
- To enhance the model's robustness to noise, the granular ball model is introduced to transform point clouds into granular ball clouds. This approach not only improves robustness but also preserves the complete shape of the point cloud.
- Moreover, due to the varying sizes of granular balls capturing multi-granularity information across different positions, this work utilizes these coarse-grained features for denoising and outlier rejection.
- Furthermore, to demonstrate the effectiveness of GRICP, extensive experiments were conducted on synthetic and real datasets.

The implementation of GRICP is available at

Code — https://github.com/little1shadow/GRICP

.

Related Work

Point Cloud Registration

Point cloud registration algorithms for point clouds are widely used. Typically, the procedure follows these steps: first, a global coarse registration method is employed to roughly align the poses of the two point clouds, followed by a fine registration method to accurately align the local surfaces. There exits various options for global coarse registration methods, such as RANSAC (Chen, Hung, and Cheng 1999), Gore (Bustos and Chin 2017) and FGR (Zhou, Park, and Koltun 2016). But fine registration techniques predominantly rely on Iterative Closest Point (ICP) algorithm (Besl and McKay 1992) and its variants. However, ICP has two main drawbacks: it is sensitive to noise and prone to getting stuck in local optima.

The mean squared error (MSE) (Marmolin 1986) is used as the loss function for ICP to iteratively minimize the Euclidean distance between pairs of closest points. Consequently, ICP is susceptible to complex non-Gaussian noises such as those from multimodal distributions. To address these limitations, robust loss functions have been studied in previous works (Bouaziz, Tagliasacchi, and Pauly 2013), (Wu et al. 2019) to reduce the influence of noisy point pairs. A p-norm is incorporated into ICP to promote sparsity in point-wise distances in (Bouaziz, Tagliasacchi, and Pauly 2013), and the Maximum Correntropy Criterion (MCC) (Liu, Pokharel, and Principe 2007) is employed as a similarity measure to lessen the impact of noise, as discussed in (Wu et al. 2019). Besides robustness, another key aspect of ICP is the convergence rate. A symmetric objective function which converges faster than MSE for ICP is proposed in (Li et al. 2022) and (Rusinkiewicz 2019). Other strategies focus on accelerating the alignment process. For example, the transformation update is treated as a fixed-point iteration problem and utilizes Anderson acceleration (Anderson 1965) to speed up convergence as outlined in (Pavlov et al. 2018) and (Zhang, Yao, and Deng 2021).

Because ICP matches the closest pair of points based on Euclidean distance as correspondences at each iteration, the resulting matches often include many outliers. This issue causes ICP to get stuck in local optima when there is a large rotational offset between the source and target point clouds. The ICP variants mentioned above do not address this problem. Among the ICP variants that aim to find the global optimum, the most notable are Global ICP (Go ICP) (Yang et al. 2015) and Deep Closest ICP (DCP) (Wang and Solomon 2019). Go ICP uses a branch-and-bound method to recursively search the entire rigid transformation space for the optimal solution, which is very time-consuming for large-scale point cloud data. DCP uses Transformers to extract semantic information from the point clouds and constructs matches based on this information.

Granular-Ball Computing

Grounded on the theoretical underpinnings of traditional granularity computation and assimilating the human cog-

nitive paradigm of "large scale first" (Chen 1982), Wang (Wang 2017) pioneered the concept of multi-granularity cognitive computation. Adhering to this methodology, Xia (Xia et al. 2019) proposed an efficient, stable, and interpretable computational approach named granular-ball computing, which utilizes granular balls to cover and represent data. This unique way enables the method to handle complex datasets with greater ease and efficiency compared to traditional point-based methods. Due to the excellent multi - granularity perception ability of the granular ball model, it has been adopted in various fields. Specifically, such as granular ball clustering (Xie et al. 2024a,b),granular-ball based classification methods (Quadir and Tanveer 2024; Xia et al. 2024b), granular-ball sampling methodologies (Xia et al. 2021), granular-ball rough sets (Xia et al. 2023; Zhang et al. 2023; Xia et al. 2020), granular-ball three-way decisions (Yang et al. 2023, 2024; Xia et al. 2024a), and reinforcement learning based on granular ball (Liu et al. 2024). Additionally, a number of applications have verified the high effectiveness of granular ball. For instance, the utilization of granular-ball in text adversarial defense (Wang et al. 2024a), label noise combating (Dai et al. 2024; Wang et al. 2024b).

Method

Convert Point Cloud to Granular Ball Cloud

Granular ball (Xia, Xie, and Wang 2022) computation is an adaptive clustering method inspired by the "large scale first" cognitive mechanism. In this study, we are given a point cloud $\mathcal{X} = \hat{x_i}(i = 1, 2...n_p)$ and use granular balls $gb_1, gb_2...gb_{n_b}$ to cover the point cloud $\mathcal{X}$. The number of points contained in each granular ball gb_j is denoted as $|gb_j|$, and the coverage degree is represented by $\sum_{j=1}^{n_b} |gb_j|/n_p$. The basic model of granular ball is as follows

$$\begin{aligned} &\min \frac{n_p}{\sum_{j=1}^{n_b}(|gb_j|)} + n_b \\ &s.t. \quad \textit{quality}(gb_j) > T \end{aligned} \tag{1}$$

where n_b denotes the number of granular balls. The operator *quality(.)* represents the ability of a granular ball to describe the characteristics of all points within it. The objective function of the granular ball model aims to use fewer high-quality granular balls to cover more points (Quadir and Tanveer 2024), thereby capturing coarse-grained information and accurately depicting the shape of the point cloud.

The quality of gb_k is defined by

$$AD_k = \frac{s_k}{n_k}, \tag{2}$$

where s_k calculated as $s_k = \sum_{i=1}^{n_k} \|x_{ki} - c_k\|$ and n_k represents the number of points inside gb_k. The term AD_k denotes the average distance and can also be interpreted as the density , denoted as d_k. The geometric center c_k of gb_k is identified as

$$c_k = \frac{\sum_{i=1}^{n_k} x_{ki}}{n_k}, r_k = max\|x_{ki} - c_k\|, i = 1, 2...n_k, \tag{3}$$

where r_k is the radius of gb_k. The criterion for a granular-ball to stop dividing is

$$\rho(AD_{k1} + AD_{k2}) > AD_k, \tag{4}$$

where ρ is the ball spliting parameter.

When the quality of two sub-granular balls gb_{k1} and gb_{k2} is lower than that of gb_k, it indicates that gb_k has achieved high quality and should stop dividing. The source point cloud $\mathcal{X}$ and the target point cloud $\mathcal{Y}$ are transformed into the source ball cloud $\mathcal{GB}_X = gb_{xi}(i = 1, 2...n_x)$ and the target ball cloud $\mathcal{GB}_Y = gb_{yi}(i = 1, 2...n_y)$ respectively, where n_x and x_y is number of granular balls.

Correspondence Generation

When registering granular ball cloud, we aim for the maximum overlap volume between ball clouds, as shown in Fig. 4(a), rather than minimizing the l_2 distance between the two balls cloud for the reason that focusing solely on the distance between the centers of two granular balls can lead to incorrect matches. For example, in Fig. 4(b), the distance between ball A and ball C is greater than that between ball A and ball B, even though ball A and ball C are better matches. But it is possible that some balls do not intersect with others. Therefore, when considering the distance between balls, we should take into account both the l_2 distance and the overlap ratio.

In Fig.5, we present the cross-section of the overlapping region of two intersecting balls in three-dimensional space, with intersection points labeled as P and Q. As shown in Fig.5, the total volume of the overlapping region $V_{overlap}$ can be expressed as:

$$V_{overlap} = \pi {h_1}^2 (r_2 - \frac{h_1}{3}) + \pi {h_2}^2 (r_1 - \frac{h_2}{3}) \tag{5}$$

The overlap ratio $R_{overlap}$ is defined as follows:

$$R_{overlap} = \begin{cases} 0, d > r_1 + r_2; \\ \frac{V_{overlap}}{\frac{4}{3}\pi max(r_1,r_2)^3}, |r_1 - r_2| <= d <= r_1 + r_2; \\ \frac{min(r_1,r_2)^3}{max(r_1,r_2)^3}, d < |r_1 - r_2|. \end{cases} \tag{6}$$

where $d = \|o_1 - o_2\|_2$. Consequently, let the reciprocal of the overlap ratio of the i-th pair of matching balls be:

$$D_{io} = \begin{cases} 0, d > r_{i1} + r_{i2}; \\ \frac{1}{R_{overlap}}, d_i <= r_{i1} + r_{i2}. \end{cases} \tag{7}$$

The goal of correspondence generation is to find the closest ball gb_{yi} in $\mathcal{GB}_Y$ for each gb_{xi} in the GB set $\mathcal{GB}_X$. Specific, for a ball gb_{xi}, its nearest ball gb_{yi} is:

$$gb_{yi} = \underset{gb_y \in \mathcal{GB}_Y}{\arg\min}\ m_1 * \|x_i - y_i\|_2 + m_2 * D_{io}(gb_{xi}, gb_y), \tag{8}$$

where m_1 and m_2 are combined weights and x_i and y_i are center points of gb_{xi}, gb_{yi}. It can be solved by $K - d$ Tree.

Outlier Rejection

Due to the use of l_2 distance and the overlap ratio to generate correspondences, a large number of incorrect correspondences can occur. To address this issue, we note that the radius of the balls and the overlap region with their neighbors can be seen as coarse-grained features. If the coarse-grained features of two matched balls (gb_{xi}, gb_{yi}) differ markedly,

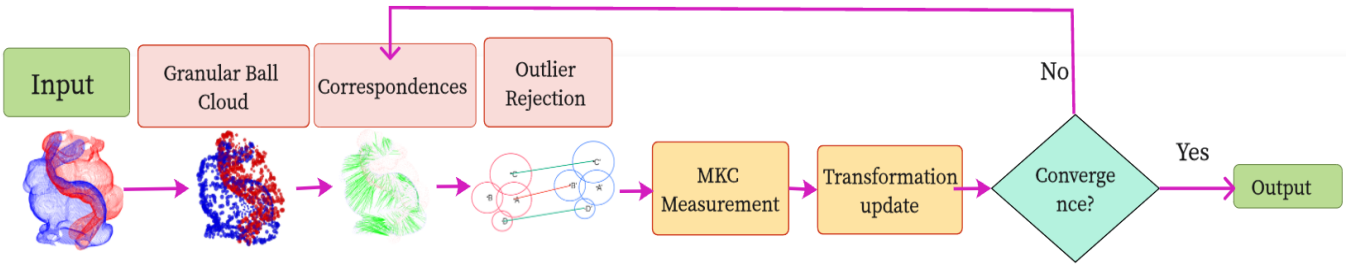

Figure 3: An overview of the proposed method. We first convert the point cloud into granular ball cloud. Then, based on these granular balls, we generate correspondences and perform outlier rejection using coarse-grained features of the granular balls. We use MKC as the loss function and derive the rigid transformation.

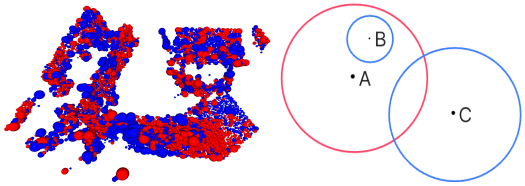

(a) (b)

Figure 4: (a) Perfect alignment result, where the overlap rate between the two granular ball clouds is maximized. (b) Granular balls in the source overlap with multiple granular balls in the target. Red represents the source, and blue represents the target.

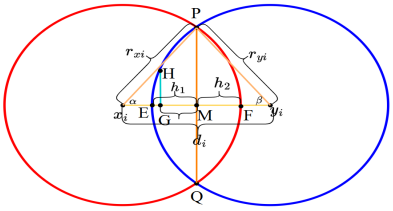

Figure 5: The calculation of overlapping volume

the correspondence is likely incorrect. First, a radius difference score is computed for each correspondence (gb_{xi}, gb_{yi}) as follows:

$$\text{score}((gb_{xi}, gb_{yi})) = \frac{|r_{xi} - r_{yi}|}{max(r_{xi}, r_{yi})}, \tag{9}$$

where r_{xi} and r_{yi} represent the radii of the correspondence (gb_{xi}, gb_{yi}). These correspondences with scores larger than a threshold τ_1 will be viewed as outliers and eliminated.

Many correspondences with low radius difference scores may still be outliers. As shown in Fig. 6, although spheres A and B' have similar sizes, it is clear that A and B' have different overlap situations with their neighbors, making $(gb_A, gb_{B'})$ an outlier. For simplicity, we use the overlap volume between the ball and its neighbors as the overlap feature. Similarly, when the difference in overlap features between two balls exceeds a threshold τ_2, the correspondence is considered an outlier.

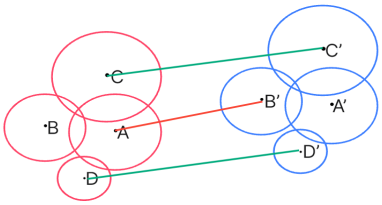

Figure 6: outlier rejection. Red lines indicate incorrect match, while green lines represent correct match.

Transformation Update

Measure the error distribution using MKC. Because both the l_2 distance and the overlap ratio is considered, the distance for the i_{th} correspondence is:

$$e_i = m_1 * D_{il} + m_2 * D_{io}, \tag{10}$$

where

$$D_{il} = \|Rx_i + t - y_i\|_2 \tag{11}$$

The $R \in \mathbb{R}^{3\times3}$ is a rigid transformation matrix, and $t \in \mathbb{R}^{3\times1}$ is a translation vector which be initialized as $R_0 = I$ and $t_0 = [0, 0, 0]^T$ respectively. The update process of the rigid transformation applying using (R_{k-1}, t_{k-1}) to estimate (R_k, t_k) to minimize the distance of point clouds until convergence.

In iteration k, the error distribution can be measured by MKC. It can be obtain:

$$(R_k, t_k) = \arg\max_{R,t} J(e) = \frac{1}{N}\sum_{i=1}^{N}\sum_{j=1}^{M}\frac{\lambda_j}{\sqrt{2\pi} * \sigma_j} exp(-\frac{(e_i - c_j)^2}{2{\sigma_j}^2}). \tag{12}$$

How to determine the free parameters $\boldsymbol{\lambda} = [\lambda_1, \lambda_2, \ldots, \lambda_M]^T$, $\boldsymbol{c} = [c_1, c_2, \ldots, c_M]^T$, and $\boldsymbol{\sigma} = [\sigma_1, \sigma_2, \ldots, \sigma_M]^T$ is studied in (Chen et al. 2021).

Reduce the number of free variables. This is a complex multi-objective optimization problem. To reduce the number of free variables, the partial derivative of the error with respect to t is given by:

$$\frac{\partial J(e))}{\partial t} = \frac{1}{N}\sum_{i=1}^{N}\sum_{j=1}^{M} w_{ij}(Rx_i + t - y_i) \tag{13}$$

where

$$w_{ij} = \begin{cases} \frac{\lambda_j(c_j - e_i)}{\sqrt{2\pi}\sigma_j^3} exp(\frac{-(e_i - c_j)^2}{2{\sigma_j}^2}) * \frac{m_1}{d_i}, \text{others ;} \\ \frac{\lambda_j \eta_i (c_j - e_i)}{\sqrt{2\pi}\sigma_j^3} exp(\frac{-(e_i - c_j)^2}{2{\sigma_j}^2}), d_i \in [|r_{i1} - r_{i2}|, r_{i1} + r_{i2}]. \end{cases} \tag{14}$$

and η_i is a constant related to the radii and distance between the two granular balls. For more details, please refer to the supplementary materials.

Let $\frac{\partial J(e)}{\partial t} = 0$, then it can be deduced:

$$t_k = \frac{\sum_{i=1}^{N}\sum_{j=1}^{M} w_{ij}(y_i - Rx_i)}{W} \tag{15}$$

where $W = \sum_{i=1}^{N}\sum_{j=1}^{M} w_{ij}$.

Substituting t in (12), It follows that:

$$\arg\max_R J(e) = \frac{1}{N}\sum_{i=1}^{N}\sum_{j=1}^{M} \frac{\lambda_j}{\sqrt{2\pi} * \sigma_j} exp(\frac{-(m_1 * D_{il} + m_2 * D_{io} - c_j)^2}{2{\sigma_j}^2}), \tag{16}$$

To simplify (16), let

$$\begin{cases} p_i = x_i - \frac{\sum_{i=1}^{N}\sum_{j=1}^{M} w_{ij}x_i}{W} \\ q_i = y_i - \frac{\sum_{i=1}^{N}\sum_{j=1}^{M} w_{ij}y_i}{W}. \end{cases} \tag{17}$$

Following this, $D_{il} = \|Rp_i - q_i\|_2$. Substituting t in D_{io} directly is complex when $d_i \in (|r_{i1} - r_{i2}|, r_{i1} + r_{i2})$, then we can multiply the numerator and denominator by $\|Rp_i - q_i\|_2$, then $D_{io} = z_i\|Rp_i - q_i\|_2$, where

$$z_i = \frac{\frac{4}{3}max(r_{i1}, r_{i2})^3}{(h_{i1}{}^2(r_{i1} - \frac{h_{i1}}{3}) + h_{i2}{}^2(r_{i2} - \frac{h_{i2}}{3}))\|Rp_i - q_i\|_2} \tag{18}$$

Then it can be deducted:

$$D_{io} = \begin{cases} 0, d > r_{i1} + r_{i2}; \\ z_i\|Rp_i - q_i\|_2, |r_{i1} - r_{i2}| <= d_i <= r_{i1} + r_{i2}; \\ \frac{max(r_{i1}, r_{i2})^3}{min(r_{i1}, r_{i2})^3}, d_i < |r_{i1} - r_{i2}| \end{cases} \tag{19}$$

For simplicity, let $m_2 \leftarrow m_2 * z_i$ when $|r_{i1} - r_{i2}| <= d_i <= r_{i1} + r_{i2}$. Then

$$J(e) = \frac{1}{N}\sum_{i=1}^{N}\sum_{j=1}^{M} \frac{\lambda_j}{\sqrt{2\pi} * \sigma_j} exp(-\frac{(a_i\|Rp_i - q_i\|_2 + b_j)^2}{2{\sigma_j}^2}), \tag{20}$$

where

$$a_i = \begin{cases} m_1, other; \\ m_1 + m_2, |r_{i1} - r_{i2}| <= d_i <= r_{i1} + r_{i2}. \end{cases}$$
$$b_j = \begin{cases} -c_j, other; \\ m_2 * \frac{max(r_{i1}, r_{i2})^3}{min(r_{i1}, r_{i2})^3} - c_j, d <= |r_{i1} - r_{i2}|. \end{cases} \tag{21}$$

Transform the nonlinear problem into a linear one. The half-quadratic technique is introduced to solve the nonlinear optimization problem (20). We can derive following proposition by convex conjugate functions (Rockafellar 2015):

suppose $g(x) \triangleq \exp(-x^2/2\sigma^2)$, there exits a convex conjugated function ϕ such that

$$g(x) = \arg\max_{u'}(u' \frac{\|x\|_2^2}{\sigma^2} - \phi(u')). \tag{22}$$

Defined:

$$S_{ij} = a_i\|Rp_i - q_i\|_2 + b_i, \quad g(s_{ij}) = \exp\left(-\frac{||s_{ij}||_2^2}{2\sigma_j^2}\right). \tag{23}$$

The conjugate function of $g(.)$ is:

$$g(s_{ij}) = u_{ij}\frac{(a_i\|Rp_i - q_i\|_2 + b_j)^2}{\sigma_j^2} - \phi(u_{ij}), \tag{24}$$

where $u_{ij} = -\exp\left(-\frac{a_i\|Rp_i - q_i\|_2 + b_j}{\sigma_j^2}\right)$

In the k-th iteration, using R_{k-1} to compute u_{ij}. Thus,

$$g(s_{ij}) = \frac{u_{ij}}{\sigma_j^2}a_i^2||Rp_i - q_i||_2^2 + \frac{u_{ij}}{\sigma_j^2}(l_{ij} + b_j^2) - \phi(u_{ij}), \tag{25}$$

where $l_{ij} = 2a_ib_j||R_{k-1}p_i - q_i||_2$ and the second and third terms are constants. Thus, It can be derived:

$$\arg\max_R J(e) = \frac{1}{N}\sum_{i=1}^{N}\sum_{j=1}^{M} \frac{\lambda_j}{\sqrt{2\pi}\sigma_j}\frac{u_{ij}}{\sigma_j^2}a_i^2(p_i^T p_i + q_i^T q_i - 2q_i^T Rp_i) \tag{26}$$

the $p_i^T p_i + q_i^T q_i$ can be seen as a constant, and setting $u_{ij} \leftarrow \frac{\lambda_j}{\sqrt{2\pi}\sigma_j}\frac{u_{ij}}{\sigma_j^2}a_i^2$, it follows that:

$$\arg\max_R J(e) = \arg\min_R \frac{1}{N}\sum_{i=1}^{N} v_i q_i^T Rp_i, \tag{27}$$

where $v_i = \sum_{j=1}^{M} u_{ij}$. Let $V_{N\times N} = \text{diag}(v_i)$, $Q_{N\times 3} = [q_1^T, q_2^T, \ldots, q_N^T]^T$, and $P_{3\times N} = [p_1, p_2, \ldots, p_N]$. Thus,

$$\arg\max_R J(e) = -\text{tr}(VQRP) = -\text{tr}(RH), \tag{28}$$

where $H = PVQ$.

Resolve R by SVD. The matrix R must fulfill two conditions: $RR^T = I$ and $\det(R) = 1$. The I represents the identity matrix, and $\det(.)$ is determinant operator. To address the objective function, the Lagrange multiplier technique is utilized. The Lagrange function is defined as

$$L(R, K, \eta) = -\text{tr}(RH) + \text{tr}(K(RR^T - I)) + \eta(\det(R) - 1), \tag{29}$$

where K is an $N \times N$ matrix and η is a constant. By computing the partial derivatives of L, we obtain:

$$\frac{\partial L}{\partial R} = -H^T + 2RK + \eta R = 0, \tag{30}$$

$$\frac{\partial L}{\partial K} = RR^T - I = 0, \tag{31}$$

$$\frac{\partial L}{\partial \eta} = \det(R) - 1 = 0. \tag{32}$$

Letting $L' = 2K + \eta I$, the above equation implies:

$$RL' = H^T. \tag{33}$$

Transposing both sides yields:

$$L'^T R^T = H. \tag{34}$$

Multiplying (33) and (34), we derive:

$$L'^T L' = L'^2 = HH^T. \tag{35}$$

Applying singular value decomposition to H, we have:

$$H = U\Lambda V. \tag{36}$$

In this scenario, U and V are orthonormal matrices, while Λ is a diagonal matrix with non-negative eigenvalues sorted in descending order. Rewriting the previous equation gives:

$$L'^2 = U\Lambda^2 U^T. \tag{37}$$

To satisfy equation (37), we construct $L' = U\Lambda D U^T$, where $D = \text{diag}(d_i)$ and d_i can be either 1 or -1. This results in:

$$\det(L') = \det(\Lambda)\det(D). \tag{38}$$

Simultaneously, from the earlier equation, we know:

$$\det(L') = \det(R)\det(H) = \det(H). \tag{39}$$

By comparing the two, we find:

$$\det(H) = \det(\Lambda)\det(D). \tag{40}$$

Thus, if $\det(H) > 0$, then $\det(D) > 0$.

$$\begin{cases} d_1 = d_2 = \cdots = d_f = -1, & \text{if } f \text{ is even;} \\ d_1 = d_2 = \cdots = d_{f-1} = -1, d_f = 1, & \text{if } sf \text{ is odd.} \end{cases}$$

Where f denotes the dimension of D. Conversely, if $\det(H) < 0$, then $\det(D) < 0$, hence

$$\begin{cases} d_1 = d_2 = \cdots = d_f = -1, & \text{if } f \text{ is odd;} \\ d_1 = d_2 = \cdots = d_{s-1} = -1, d_f = 1, & \text{if } f \text{ is even.} \end{cases}$$

Finally, substituting $L'^{-1} = (U\Lambda D U^T)^{-1} = U\Lambda^{-1}D^{-1}U^T$ into the equation (33), the rotation for the k-th iteration is given by

$$R_k = H^T L'^{-1} = (V\Lambda U^T)(U\Lambda^{-1}D^{-1}U^T) = VDU^T. \tag{41}$$

Thus, R_k can be calculated. Updating t_k with R_k, we get

$$t_k = \frac{\sum_{i=1}^{N}\sum_{j=1}^{M} w_{ij}(y_i - R_k x_i)}{W} \tag{42}$$

Experiments

Experimental Settings

Compared methods and evaluation metrics. The GRICP was compared with various ICP variants, including standard ICP (Besl and McKay 1992), Sparse ICP (Bouaziz, Tagliasacchi, and Pauly 2013), AA ICP (Rusinkiewicz 2019), Fast ICP (Zhang, Yao, and Deng 2021), Robust ICP (Zhang, Yao, and Deng 2021), Go ICP (Yang et al. 2015), and FGR (Zhou, Park, and Koltun 2016). Rotation error (RE) and translation error (TE) were computed to quantify the performance of each algorithm across different scenarios.

The computation of RE and TE is performed as

$$\begin{aligned} RE(\hat{R}) &= arccos\frac{Tr(\hat{R}^T R^*) - 1}{2}, \\ TE(\hat{t}) &= \|\hat{t} - t^*\|_2, \end{aligned} \tag{43}$$

where $\hat{R}$ and $\hat{t}$ is the transformation computed, R^* and t^* is ground-truth rotation and translation.

Method	100°		120°		150°		180°	
	RE	TE	RE	TE	RE	TE	RE	TE
ICP	3.064	0.302	3.049	0.305	3.050	0.293	3.009	0.148
AAICP	2.587	0.291	2.772	0.302	3.051	0.278	3.136	0.152
FICP	3.055	0.302	3.049	0.305	3.050	0.293	3.009	0.148
RICP	3.114	0.297	3.132	0.298	3.135	0.257	3.133	0.133
SICP	2.516	0.156	2.936	0.152	2.510	0.091	3.120	0.206
GoICP	0.031	0.011	0.082	0.016	**0.012**	**0.013**	0.005	**0.014**
FGR	0.804	0.058	0.324	0.069	0.767	0.076	1.050	0.174
Ours	**0.008**	**0.002**	**0.006**	**0.003**	0.036	0.017	**0.001**	0.019

Table 1: Registration Results under large rotational offsets in Stanford 3D Scanning Repository and 3DMatch.

Datasets. The experiments utilized two primary datasets: synthetic data from the Stanford 3D Scanning Repository (Levoy et al. 2005) like bunny, dragon and real data from 3DMatch (Zeng et al. 2017) like BA, cloud_bin. To comprehensively evaluate performance, the experimental design covered multiple scenarios, including large-scale rotational offsets, partial overlaps, and Gaussian noise.

Implementation details. We set the granular ball splitting parameter ρ to 0.78, and the outlier rejection parameters τ_1 and τ_2 to 0.1. The weights for the correspondence distance, m_1 and m_2, are set to 0.9 and 0.1, respectively. The model is executed on an Intel® Core i5-10300H CPU @ 2.50GHz.

Datasets	FPFH	GB
3DMatch(no noise)	**0.4196**	0.3848
3DMatch(10% noise)	0.2897	**0.3536**
3DMatch(20% noise)	0.2124	**0.3218**
3DMatch(30% noise)	0.1833	**0.2825**
3DMatch(50% noise)	0.1378	**0.2385**
3DScanRepo(no noise)	**0.7489**	0.7113
3DScanRepo(10% noise)	**0.6992**	0.6915
3DScanRepo(20% noise)	0.6879	**0.6884**
3DScanRepo(30% noise)	0.6526	**0.6716**
3DScanRepo(50% noise)	0.6027	**0.6346**

Table 2: Precision comparison of GB and FPFH in generating correspondences

Comparison Evaluation

According to (Li et al. 2020), the maximum allowable rotation angle of ICP is 90°. Therefore, for each model, we evaluated the performance under rotational offsets of 100°, 120°, 150°, and 180°. From Table 1, it can be observed that our method achieves good performance in terms of registration with large rotation offsets.

For partial overlap environment, we conducted experiments on the Stanford 3D Scanning Repository with four

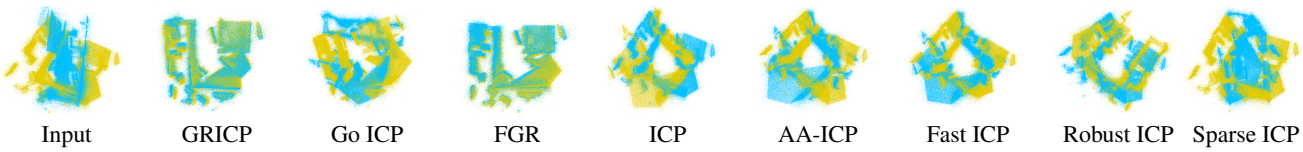

Figure 7: Registration results Compared with other methods.

Method	60% overlap		70% overlap		80% overlap		90% overlap	
	RE	TE	RE	TE	RE	TE	RE	TE
ICP	2.778	0.179	2.748	0.165	2.773	0.147	2.750	0.163
AAICP	3.061	0.160	2.876	0.150	2.914	0.122	2.971	0.138
FICP	2.778	0.179	2.748	0.164	2.773	0.147	2.750	0.163
RICP	2.852	0.247	2.782	0.151	2.782	0.176	2.714	0.158
SICP	3.058	0.183	3.092	**0.119**	3.073	0.135	3.134	0.131
GoICP	2.104	0.558	2.962	0.413	**0.031**	0.022	0.030	0.016
FGR	1.744	0.169	1.743	0.164	1.744	0.163	1.743	0.163
Ours	**0.412**	**0.125**	**0.308**	0.145	0.143	**0.015**	**0.030**	**0.015**

Table 3: Registration Results with Partial Overlap on Stanford 3D Scanning Repository.

overlap rates: 60%, 70%, 80%, and 90%. From the Table 3, one can see that our method can obtain the lowest error.

Method	10% noise		20% noise		30% noise		50% noise	
	RE	TE	RE	TE	RE	TE	RE	TE
ICP	0.349	0.158	2.907	0.145	2.948	0.154	2.976	0.158
AAICP	0.624	0.151	2.713	0.150	2.679	0.148	2.179	0.162
FICP	0.623	0.151	2.712	0.151	2.652	**0.141**	2.187	0.168
RICP	0.349	0.158	3.101	0.139	3.087	0.149	2.848	0.128
SICP	2.253	0.167	1.413	0.166	1.650	0.169	1.916	0.167
GoICP	**0.185**	0.159	0.476	0.158	2.882	0.173	1.979	0.201
FGR	1.606	0.600	0.208	0.052	0.062	**0.146**	**0.176**	0.127
Ours	0.287	**0.150**	**0.101**	**0.046**	**0.044**	0.162	0.238	**0.124**

Table 4: Registration Results under Gaussian Noise on 3DMatch.

To demonstrate the robustness of GRICP, we explored the registration results on 3DMatch by adding 10%, 20%, 30%, and 50% Gaussian noise which standard deviations are 0.01, 0.02, 0.03, and 0.05. As shown in Table 4, GRICP can withstand different degrees of noise.

In contrast, Go ICP performs poorly when there is a high level of noise due to that the shape of the point cloud becomes blurred.

Sensitivity Study on the Hyperparameters of GB

In this section, we examine the impact of outlier rejection parameters τ_1 and τ_2 on registration results. From Fig. 8,

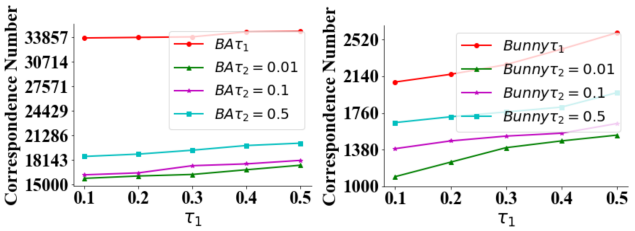

Figure 8: Sensitivity Analysis of Outlier Rejection Parameters.(a): BA model. (b): Bunny model.

Datasets	GRICP	GOICP	FGR	ICP	AAICP	FICP	RICP	SICP
3DScanRepo	0.10	4.21	0.61	0.003	0.002	0.007	0.009	0.008
3DMatch	2.86	599.08	534	0.072	0.058	0.127	0.150	0.087

Table 5: Comparison of run time (in seconds).

the results indicate that using both radius and overlap ratio for outlier rejection greatly eliminates most incorrect correspondences. Moreover, this outlier removal strategy does not exhibit notable sensitivity to the values of τ_1 and τ_2. When these two parameters are within the range [0.01-0.5], the number of correspondences does not change noticeably.

In Table 2, we compared the performance of the Granular Ball (GB) method and Fast Point Feature Histogram (FPFH) (Rusu, Blodow, and Beetz 2009) in generating correspondences. FPFH excels in producing high-quality correspondences under noise-free conditions but is sensitive to noise. In contrast, the GB method demonstrates robustness to noise. Table 5 shows the efficiency of GRICP compared with GO ICP and FGR.

Conclusion

We propose a global and robust ICP framework called GRICP. The GRICP convert point clouds into granular ball clouds, applying the coarse features of these granular balls for removing outliers. MKC is introduced as the loss function to evaluate the error distribution, with the goal of achieving the global optimum. To showcase the performance of GRICP, we performed thorough experiments on both synthetic and real datasets under three different scenarios: large-scale rotation, partial overlap, and Gaussian noise. The results demonstrate the effectiveness of GRICP in complex registration scenarios. Moreover, hyperparameter analysis confirms that GRICP shows generalization capabilities.

Acknowledgements

This work was supported by the National Science Foundation of China(Grant Nos.62222601, 62450043, 62176033, 622221005, 61936001)

References

Agarwal, S.; Furukawa, Y.; Snavely, N.; Simon, I.; Curless, B.; Seitz, S. M.; and Szeliski, R. 2011. Building rome in a day. *Communications of the ACM*, 54(10): 105–112.

Anderson, D. G. 1965. Iterative procedures for nonlinear integral equations. *Journal of the ACM (JACM)*, 12(4): 547–560.

Besl, P. J.; and McKay, N. D. 1992. Method for registration of 3-D shapes. In *Sensor fusion IV: control paradigms and data structures*, volume 1611, 586–606. Spie.

Bouaziz, S.; Tagliasacchi, A.; and Pauly, M. 2013. Sparse iterative closest point. In *Computer graphics forum*, volume 32, 113–123. Wiley Online Library.

Bresson, G.; Alsayed, Z.; Yu, L.; and Glaser, S. 2017. Simultaneous localization and mapping: A survey of current trends in autonomous driving. *IEEE Transactions on Intelligent Vehicles*, 2(3): 194–220.

Bustos, A. P.; and Chin, T.-J. 2017. Guaranteed outlier removal for point cloud registration with correspondences. *IEEE transactions on pattern analysis and machine intelligence*, 40(12): 2868–2882.

Chen, B.; Xie, Y.; Wang, X.; Yuan, Z.; Ren, P.; and Qin, J. 2021. Multikernel correntropy for robust learning. *IEEE Transactions on Cybernetics*, 52(12): 13500–13511.

Chen, C.-S.; Hung, Y.-P.; and Cheng, J.-B. 1999. RANSAC-based DARCES: A new approach to fast automatic registration of partially overlapping range images. *IEEE Transactions on Pattern Analysis and Machine Intelligence*, 21(11): 1229–1234.

Chen, L. 1982. Topological structure in visual perception. *Science*, 218(4573): 699–700.

Cheng, D.; Li, Y.; Xia, S.; Wang, G.; Huang, J.; and Zhang, S. 2023. A fast granular-ball-based density peaks clustering algorithm for large-scale data. *IEEE Transactions on Neural Networks and Learning Systems*.

Dai, D.; Zhu, H.; Xia, S.; and Wang, G. 2024. Granular-ball Representation Learning for Deep CNN on Learning with Label Noise. *arXiv preprint arXiv:2409.03254*.

Durrant-Whyte, H.; and Bailey, T. 2006. Simultaneous localization and mapping: part I. *IEEE robotics & automation magazine*, 13(2): 99–110.

Levoy, M.; Gerth, J.; Curless, B.; and Pull, K. 2005. The Stanford 3D Scanning Repository. http://www-graphics.stanford.edu/data/3dscanrep.

Li, J.; Hu, Q.; Zhang, Y.; and Ai, M. 2022. Robust symmetric iterative closest point. *ISPRS Journal of Photogrammetry and Remote Sensing*, 185: 219–231.

Li, P.; Wang, R.; Wang, Y.; and Tao, W. 2020. Evaluation of the ICP algorithm in 3D point cloud registration. *IEEE access*, 8: 68030–68048.

Liu, J.; Jianye, H.; Ma, Y.; and Xia, S. 2024. Unlock the Cognitive Generalization of Deep Reinforcement Learning via Granular Ball Representation. In *Forty-first International Conference on Machine Learning*.

Liu, W.; Pokharel, P. P.; and Principe, J. C. 2007. Correntropy: Properties and applications in non-Gaussian signal processing. *IEEE Transactions on signal processing*, 55(11): 5286–5298.

Marmolin, H. 1986. Subjective MSE measures. *IEEE transactions on systems, man, and cybernetics*, 16(3): 486–489.

Pavlov, A. L.; Ovchinnikov, G. W.; Derbyshev, D. Y.; Tsetserukou, D.; and Oseledets, I. V. 2018. AA-ICP: Iterative closest point with Anderson acceleration. In *2018 IEEE international conference on robotics and automation (ICRA)*, 3407–3412. IEEE.

Quadir, A.; and Tanveer, M. 2024. Granular ball twin support vector machine with pinball loss function. *IEEE Transactions on Computational Social Systems*.

Rockafellar, R. T. 2015. Convex analysis:(pms-28).

Rusinkiewicz, S. 2019. A symmetric objective function for ICP. *ACM Transactions on Graphics (TOG)*, 38(4): 1–7.

Rusu, R. B.; Blodow, N.; and Beetz, M. 2009. Fast point feature histograms (FPFH) for 3D registration. In *2009 IEEE international conference on robotics and automation*, 3212–3217. IEEE.

Wang, G. 2017. DGCC: data-driven granular cognitive computing. *Granular Computing*, 2(4): 343–355.

Wang, Y.; and Solomon, J. M. 2019. Deep closest point: Learning representations for point cloud registration. In *Proceedings of the IEEE/CVF international conference on computer vision*, 3523–3532.

Wang, Z.; Li, J.; Xia, S.; Lin, L.; and Wang, G. 2024a. Text Adversarial Defense via Granular-Ball Sample Enhancement. In *Proceedings of the 2024 International Conference on Multimedia Retrieval*, 348–356.

Wang, Z.; Zhang, T.; Xia, S.; Lin, L.; and Wang, G. 2024b. GB: Combating Textual Label Noise by Granular-ball based Robust Training. In *ICMR*.

Wu, Z.; Chen, H.; Du, S.; Fu, M.; Zhou, N.; and Zheng, N. 2019. Correntropy based scale ICP algorithm for robust point set registration. *Pattern Recognition*, 93: 14–24.

Xia, D.; Wang, G.; Zhang, Q.; Yang, J.; and Xia, S. 2024a. Three-way approximations fusion with granular-ball computing to guide multi-granularity fuzzy entropy for feature selection. *IEEE Transactions on Fuzzy Systems*.

Xia, S.; Lian, X.; Wang, G.; Gao, X.; Chen, J.; and Peng, X. 2024b. Gbsvm: an efficient and robust support vector machine framework via granular-ball computing. *IEEE Transactions on Neural Networks and Learning Systems*.

Xia, S.; Liu, Y.; Ding, X.; Wang, G.; Yu, H.; and Luo, Y. 2019. Granular ball computing classifiers for efficient, scalable and robust learning. *Information Sciences*, 483: 136–152.

Xia, S.; Wang, C.; Wang, G.; Gao, X.; Ding, W.; Yu, J.; Zhai, Y.; and Chen, Z. 2023. GBRS: A Unified Granular-Ball Learning Model of Pawlak Rough Set and Neighborhood Rough Set. *IEEE Transactions on Neural Networks and Learning Systems*.

Xia, S.; Xie, J.; and Wang, G.-Y. 2022. An adaptive granularity clustering method based on hyper-ball. *CoRR*.

Xia, S.; Zhang, H.; Li, W.; Wang, G.; Giem, E.; and Chen, Z. 2020. GBNRS: A novel rough set algorithm for fast adaptive attribute reduction in classification. *IEEE Transactions on Knowledge and Data Engineering*, 34(3): 1231–1242.

Xia, S.; Zheng, S.; Wang, G.; Gao, X.; and Wang, B. 2021. Granular ball sampling for noisy label classification or imbalanced classification. *IEEE Transactions on Neural Networks and Learning Systems*, 34(4): 2144–2155.

Xie, J.; Dai, M.; Xia, S.; Zhang, J.; Wang, G.; and Gao, X. 2024a. An Efficient Fuzzy Stream Clustering Method Based on Granular-Ball Structure. In *2024 IEEE 40th International Conference on Data Engineering (ICDE)*, 901–913. IEEE.

Xie, J.; Xiang, X.; Xia, S.; Jiang, L.; Wang, G.; and Gao, X. 2024b. MGNR: A Multi-Granularity Neighbor Relationship and Its Application in KNN Classification and Clustering Methods. *IEEE Transactions on Pattern Analysis and Machine Intelligence*.

Xie, Q.; Zhang, Q.; Xia, S.; Zhao, F.; Wu, C.; Wang, G.; and Ding, W. 2024c. Gbg++: A fast and stable granular ball generation method for classification. *IEEE Transactions on Emerging Topics in Computational Intelligence*.

Yang, J.; Li, H.; Campbell, D.; and Jia, Y. 2015. Go-ICP: A globally optimal solution to 3D ICP point-set registration. *IEEE transactions on pattern analysis and machine intelligence*, 38(11): 2241–2254.

Yang, J.; Liu, Z.; Xia, S.; Wang, G.; Zhang, Q.; Li, S.; and Xu, T. 2024. 3WC-GBNRS++: A novel three-way classifier with granular-ball neighborhood rough sets based on uncertainty. *IEEE Transactions on Fuzzy Systems*.

Yang, X.; Li, Y.; Xia, S.; Lian, X.; Wang, G.; and Li, T. 2023. Granular-Ball Three-Way Decision. In *International Joint Conference on Rough Sets*, 283–295. Springer.

Zeng, A.; Song, S.; Nießner, M.; Fisher, M.; Xiao, J.; and Funkhouser, T. 2017. 3DMatch: Learning Local Geometric Descriptors from RGB-D Reconstructions. In *CVPR*.

Zhang, J.; Yao, Y.; and Deng, B. 2021. Fast and robust iterative closest point. *IEEE Transactions on Pattern Analysis and Machine Intelligence*, 44(7): 3450–3466.

Zhang, Q.; Wu, C.; Xia, S.; Zhao, F.; Gao, M.; Cheng, Y.; and Wang, G. 2023. Incremental learning based on granular ball rough sets for classification in dynamic mixed-type decision system. *IEEE Transactions on Knowledge and Data Engineering*, 35(9): 9319–9332.

Zhou, Q.-Y.; Park, J.; and Koltun, V. 2016. Fast global registration. In *Computer Vision–ECCV 2016: 14th European Conference, Amsterdam, The Netherlands, October 11-14, 2016, Proceedings, Part II 14*, 766–782. Springer.